

COMBUSTION DIAGNOSTICS: PLANAR IMAGING TECHNIQUES

RONALD K. HANSON

*Department of Mechanical Engineering
Stanford University, Stanford, CA 94305*

New measurement techniques based on planar (2-d) imaging of scattered light provide a powerful complement to single-point laser-based diagnostics, with significant potential to impact combustion research. Though still in an early stage of development, these imaging methods offer prospects for non-invasive, spatially and temporally resolved measurements of species concentrations and mole fractions, temperature, density, velocity, and pressure. Imaging processes encompassed in this review include laser-induced fluorescence and Raman, Mie and Rayleigh scattering. Extensions of these 2-d techniques to new flowfield variables and species, and to 3-d imaging by rapid scanning of the illumination plane, are already in progress.

Introduction

Although flow visualization is regarded as a well developed field, with a long history of important contributions to fluid mechanics and combustion, remarkable advances in measurement capability have occurred in the past few years. Particularly noteworthy has been the development of spectroscopy-based techniques which combine species specificity with the capability for simultaneous, spatially resolved measurements at a large number of points within a plane, in essence providing two-dimensional (2-d) images of flowfield properties. These new techniques generally utilize sheet illumination from a tunable, pulsed laser source with right-angle detection of scattered light using a solid-state array detector. The detector may be coupled directly to a laboratory computer for fast storage, processing and display of planar image data. Techniques based on laser-induced fluorescence as well as Raman, Rayleigh and Mie scattering have been reported, yielding measurements of species concentration or mole fraction, temperature, density, velocity, and even pressure. Temporal resolution is generally controlled by the laser source, with 5–10 nsec pulse lengths being typical. Spatial resolution is set by the array detector, with 100×100 arrays, and hence 10,000 pixels, currently being common, though arrays with several hundred thousand and even one million pixels are now available. The extension of 2-d imaging to three dimensions using a rapidly scanned illumination plane is already in progress.

The history of this field, at least in the combustion community, is quite brief, with nearly all of the progress having been made

since Eckbreth's review¹ of spatially resolved, single-point laser diagnostics at this meeting six years ago. Several research laboratories have made important contributions, but the pioneering work on the use of planar array detection was done at Yale University with initial emphasis on Mie² and Rayleigh³ scattering. The important extension to imaging based on laser-induced fluorescence (LIF) was made nearly simultaneously by groups at Lund Institute of Technology,⁴ SRI International⁵ and Stanford University.⁶ More recently, imaging based on Raman scattering has been demonstrated at Sandia Laboratories,⁷ and LIF imaging from evaporating spray droplets has been reported⁸ by collaborators from United Technologies Research Center and the University of Texas at Dallas. Finally, the extension of LIF imaging to sense velocity has been reported by researchers at Princeton⁹ and Stanford University.¹⁰ The continued high level of activity at these and other laboratories promises to yield rapid progress in this new field, although significant research challenges remain.

The potential of imaging diagnostics in studies of combustion phenomena is readily apparent. The techniques should find extensive use for qualitative purposes, for example in surveying complex flows and in guiding development of realistic flow models, as well as for quantitative flowfield analysis. Detailed study of large- and small-scale features of flowfields will be enabled, for both reacting and nonreacting cases, as well as fundamental studies aimed at developing improved reacting-flow turbulence models. Although optical access may be a problem in some cases, imaging diagnostics may be expected to reveal previously unobserved

phenomena in the complex flowfields of practical devices. Reexamination of flowfields previously studied with traditional line-of-sight visualization methods and single-point diagnostics should also lead to observations of previously masked flow features and, ultimately, to improved understanding of the fluid mechanics.

Progress in the development of flowfield imaging is tightly coupled to advances in laser sources and, particularly, in array detector technology. In the case of lasers, the need is for higher power, higher repetition rates and broader wavelength tunability, for example providing convenient access to ultraviolet wavelengths needed to excite chemically stable compounds. As regards array detectors, the need is for improved noise performance, broader wavelength coverage (again to facilitate uv operation), and of course faster and larger arrays (more pixels). The anticipated availability of large arrays with capability for rapid, on-chip transfer of image data will also be important in establishing high-repetition-rate imaging. Since image intensification is commonly employed, there is also a requirement for improved multi-channel-plate intensifiers. Finally, cost reductions of imaging equipment are critical if these techniques are to be employed in a greater number of laboratories.

Although the aim of this paper is to provide an overview of planar imaging diagnostics relevant to combustion, the emphasis will be on LIF-based approaches, which currently offer higher sensitivity for species measurements and greater versatility for measuring multiple flowfield parameters. Example results will be presented for each of the major current LIF-imaging concepts, and also for representative Raman, Rayleigh, and Mie imaging, with the objective of illustrating both current capability and the future potential of these methods.

Laser-Induced Fluorescence

Introduction

Laser-induced fluorescence is a well-established, sensitive technique for detecting population densities of atoms and molecules in specific quantum states. Although LIF was used initially in studies of spectroscopy and chemical analysis, it is now also recognized as a powerful fluid mechanics diagnostic with the potential for monitoring flowfield parameters such as mixture mole fractions, density, temperature, velocity and pressure. The development of LIF methods has, until recently, been driven by single-point measurements, but the underlying

concepts carry over directly to multiple-point planar imaging.

The principles of LIF are well known (see Refs. 11–13 and articles cited therein for an up-to-date review) and need not be repeated in detail here. In brief, a laser source is tuned to excite a specific electronic absorption transition in the species of interest. Following the absorption process, collisional redistribution in the electronically excited state may occur prior to either collisional quenching or radiative deexcitation (fluorescence) of the molecule back to a lower electronic state. The emission, which occurs over a range of wavelengths, is usually collected at right angles and filtered spectrally at the photodetector. For a given species, the variables in the LIF process are the transition pumped, the detection spectral bandpass, the spectral intensity of the laser, and, in the case of a narrow-bandwidth laser, the location of excitation within the absorption line profile. LIF may be thought of as spatially resolved absorption, with the intersection of the illumination and collection beam paths controlling the spatial resolution of the measurement. In the case of sheet beam illumination and detection with an array detector, the size of the detector pixels and the magnification of the collection optics controls the size of the measurement volume at each image “point.”¹⁴

The governing equation for the LIF signal, S , based on a simple two-level model with weak (unsaturated) excitation, for a single detector pixel, is:^{11–16}

$$S = C E V N_s B F_{ij}(T) [A/(A + Q)] \quad (1)$$

Here, C is a group of constants specific to the experimental set-up, E is the laser energy per pulse per unit area per unit frequency, V is the measurement volume for the detector element, N_s is the number density of the absorbing species, F_{ij} is the population fraction for the pumped state, B is the Einstein coefficient for absorption, and A is the appropriate (for the transitions monitored) Einstein coefficient for spontaneous emission. The parameter Q represents the sum rate of all other transfer processes which eliminate emission into the detection bandwidth. In the most common case, with broadband collection and no chemical or pre-dissociative removal from the upper electronic state, $Q(X_i, P, T)$ is simply the electronic quench rate, which in general depends on temperature, composition through the mole fractions X_i , and pressure. Procedures for dealing with system calibration and variations in the quench rate are discussed in Refs. 14–16.

A schematic diagram of a typical experimen-

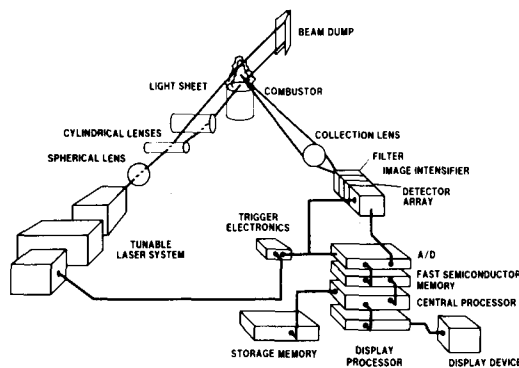


FIG. 1. Schematic diagram of typical experimental set-up for PLIF imaging.

tal set-up for planar LIF imaging (PLIF) is shown in Fig. 1. Briefly, a tunable laser source, usually pulsed, is used together with simple lenses to provide sheet illumination in the flowfield of interest. Fluorescent light from a segment of this plane is collected at right angles and imaged either directly onto the array detector or onto the front face of an image intensifier.¹⁴ Detectors currently employed are photodiode arrays,^{14,15} low-light-level vidicon cameras,¹⁶ and CCD (charge-coupled device) arrays,¹⁷ with the latter offering superior potential performance in terms of noise, linear dynamic range and spatial resolution. Image intensification is needed when the fluorescence intensity is low relative to the detection limit of the array detector, with proximity-focussed, micro-channel-plate intensifiers providing the best choice for imaging applications.¹⁴

Species Imaging

The bulk of fluorescence imaging activity has been concerned with species concentration or mole fraction measurements. A good example of such work is shown in Fig. 2 (from Refs. 18 and 19) which contrasts laser schlieren visualization with PLIF imaging of NO₂ and OH in a combustion-torch ignition study. In this experiment, a lean methane-air mixture, near the flammability limit, was first ignited in a small cylindrical prechamber. The high temperature combustion products exit from the prechamber through a circular orifice as a jet, leading to ignition and flame propagation in the main chamber. While the line-of-sight schlieren technique is useful, in this symmetrical flow, for following the high-temperature interface between unburned reactants and the burned combustion products in the torch, it provides little direct information on the combustion

chemistry and hence the possible coupling between chemistry and fluid motion. Further, the spatial resolution of schlieren visualization is limited in highly turbulent flows. The observation of OH by PLIF, on the other hand, serves as a clear indicator of the chemical reaction front of the flame and the subsequent effect of fluid motion on the state of the burned gases, and this method retains its spatial resolution in turbulent flowfields. The objective of the NO₂ imaging is to track the non-reacted gases, and this was accomplished by seeding the air with a low, chemically nonperturbing level (700 ppm) of NO₂ which decomposes rapidly (primarily by H-atom attack) in the flame zone. Thus the NO₂ imaging provides a complement to OH imaging, useful up to about 700 K where dissociation begins to occur.¹⁹

The size of the region viewed by the 12 mm × 12 mm intensified-silicon-intensified-target (ISIT) vidicon camera was 60 mm × 60 mm, while the thickness of the laser sheet was 1 mm. The NO₂ was pumped with 100 mJ at 532 nm, derived from a frequency-doubled Nd:YAG laser, while the OH was excited with 4 mJ of frequency-doubled dye laser radiation at 284.3 nm ($Q_2(9)$) transition. Gated detection (0.4 microseconds) was used with a 100×100 pixel format on the vidicon, yielding single-shot detection limits of about 70 ppm and 60 ppm for NO₂ and OH respectively.^{18,19} The measurements of NO₂ and OH were not made simultaneously, but can be compared directly because of the reproducibility of the flow.

The use of NO₂ as a flow tracer is quite attractive because of the range of possible excitation wavelengths (400–650 nm) in the visible and hence the relative ease of laser selection. For example, it should be possible to use a high-repetition-rate (5–15 kHz) metal vapor laser together with PLIF imaging for monitoring the real-time evolution of flow phenomena. By comparison, imaging of OH requires a near-uv laser, typically at 285–310 nm, and has thus far been limited to a 10 Hz repetition rate (set by the Nd:YAG pump lasers employed), although measurements up to 250 or 500 Hz should be feasible using an excimer laser either for direct excitation at 308 nm or for dye laser pumping. It should be noted, however, that high-speed imaging will require improvements in the recording rate of solid-state cameras, which are currently limited to about 500 Hz. One possibility would be to employ on-chip storage of multiple images on large detector arrays.²⁰ If intensification is employed, special short-lived phosphors will be required on the output face of the intensifier.

A second example of PLIF species imaging is

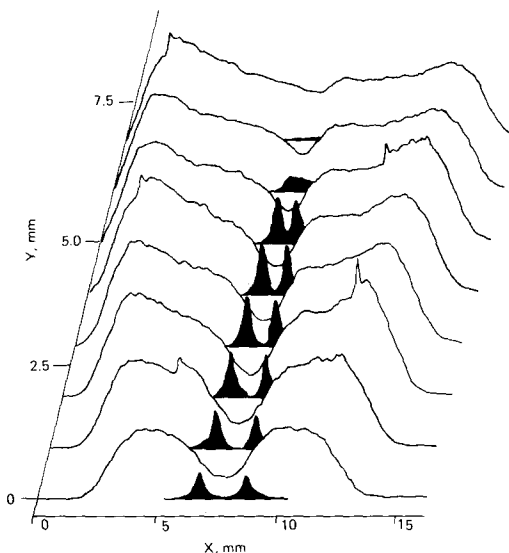


FIG. 3. Composite results from CH and OH PLIF imaging in a torch. The lines represent the OH distribution, and the filled-in profiles are for CH (Ref. 21).

provided in Fig. 3 which shows composite results of CH and OH imaging experiments (not performed simultaneously) in a small glassblowing torch.²¹ In the case of OH, a Nd:YAG-pumped dye laser at 310.7 nm was used to excite the $P_1(6)$ line of the (0,0) band, while for CH an excimer-pumped dye laser at 431.5 nm was used to pump overlapping lines in the (0,0) band. In both experiments the laser energy was about 1 mJ and broadband collection, including elastically scattered light, was employed. The important point to be made about these measurements is that the OH and CH distributions provide different and complementary information about the flame flowfield. The OH is an indicator of where already burned gases are located, i.e. where combustion has occurred, while CH marks the location of the thin, instantaneous reaction zone. The OH signals were about ten times those of CH, and both the OH and CH signals were averaged over 7 laser pulses.

A similar use of CH and OH imaging to probe burning and burned gases in a small-scale spray flame has also been reported.^{22,23} Figures 4 and 5 present sample results obtained with single-shot imaging and an intensified, 100×100 photodiode array camera. A Nd:YAG-pumped dye laser was used in both cases, with energies per pulse in the range 10–15 mJ. In order to discriminate against elastic scattering from the droplets present, OH was pumped at the $Q_1(6)$ transition of

the (1,0) band, at 283 nm, and the fluorescence from the (1,1) band was collected. The diagonal nature of CH transitions required excitation (426 nm) and detection (431.5 nm) within the same (0,0) band using a custom 3-cavity filter with 1 nm halfwidth. Further details of the experiment may be found in Refs. 22 and 23.

The results shown in Fig. 4 provide information on the instantaneous distribution of OH in the central plane of the turbulent heptane-air spray flame. The air-atomizing siphon nozzle is just below the $8 \text{ cm} \times 8 \text{ cm}$ field of view. Peak concentrations of OH (about 1000 ppm) are found in two distinct zones of combustion: a thin sheath flame at the periphery of the spray, and an interior, distributed reaction zone located above the primary fuel vaporization zone. Results obtained with increasing air flow rates showed diminishing scale size in the turbulent structures.^{22,23} The results for CH shown in Fig. 5 are for a smaller-size zone, $1.2 \text{ cm} \times 1.2 \text{ cm}$, located at the tip of the primary reaction zone. A portion of the elastically scattered light has been transmitted to enable the simultaneous display of droplet positions within the burning region marked by CH. The instantaneous flame zone is seen to have a continuous, thin filamentary structure which encompasses most of the local droplets; the maximum CH level is estimated at 100 ppm. Similar results have also been reported in gaseous flames using C₂ and CH imaging of instantaneous flame zones.²⁴ Since only a single laser source was available in these studies, the imaging of CH and OH (or C₂) was not performed simultaneously, but two-laser, dual-species (OH and C₂) imaging has been reported previously using a 1-d diode array,²⁵ and work is currently in progress on simultaneous PLIF imaging.²⁶

In the results cited thus far, and in nearly all past work to develop LIF, the species have been chemical intermediates or otherwise reactive and hence not suited for many fluid mechanics imaging applications. Exceptions which have seen some use are NO^{27,28} and biacetyl,^{29,30} and, quite recently, O₂.³¹ The extension of LIF imaging to O₂ is of course quite important, both for combustion and fluid mechanics applications, and has recently been demonstrated using both 2-d³² and 1-d³³ array detectors. The laser excitation of O₂ is carried out in the *uv* (Schumann-Runge band system, $B \leftarrow X$) and is highly temperature sensitive³⁴ as a result of the much larger Franck-Condon factors associated with absorption transitions from excited vibrational levels of ground state O₂. An argon fluoride (ArF) laser at 193 nm seems to be a particularly attractive excitation source,³² owing to the large energy per pulse (hundreds of mJ)

and high repetition rates available (500 Hz), and to system simplicity, though fairly complex spectroscopic calculations are needed to predict the fluorescence when a standard broadband laser is used.³⁴ The fact that the *B* state of O₂ is predissociated leads to a reduction in the fluorescence yield,^{31,34} but, more importantly, it also removes the usual dependence of the fluorescence signal on the mixture- and temperature-dependent quenching rate.

An example result of O₂ imaging in a combustion flow using single-pulse broadband ArF laser excitation is shown in Fig. 6.³² The 5 cm × 5 cm region imaged was located on the central vertical plane of a fuel-rich (CH₄-air) Meker-burner flame. The laser beam is incident from left-to-right, with sufficient attenuation to give an apparent asymmetry to the flowfield. As expected, the image shows a high level of O₂ upstream of the inner conical flame, since the premixed fuel and air have not yet burned, and a second zone of high signal at the outer diffusion flame where air contacts the rich products of the inner flame. It is important to realize that the signal level is a function of both O₂ mole fraction and temperature, and that a separate measurement would be needed to deconvolve these two effects. The preferred approach would appear to be to employ either a tunable, narrow-linewidth ArF laser or a two-laser/two-detection-channel arrangement. The latter should enable simultaneous determination of O₂ and temperature.

Species Imaging (Multi-Photon Excitation)

Recently multi-photon LIF has been adopted as a means of exciting species not accessible with single-photon excitation, particularly those which have their resonance transitions in the vuv region. Although the absorption process is weaker than with allowed single-photon processes, satisfactory LIF signals can be generated, in some cases, using intense laser sources together with multi-pass optical arrangements. There are some disadvantages to multi-photon excitation, associated primarily with the nonlinear dependence of the signal on illumination intensity and some uncertainties in the critical processes which must be included in a proper LIF model, but these are outweighed by the importance of gaining access to critical atomic and molecular species. Thus far, this approach has been demonstrated in combustion flows for atomic O^{35,36} and H³⁶ using intensified 1-d (linear) array detection, and CO using both 1-d³⁷ and 2-d^{38,39} arrays for imaging.

Example results³⁶ for H- and O-atom imag-

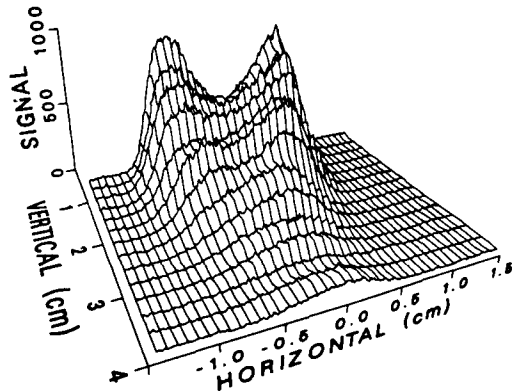


FIG. 7. Mapping of atomic hydrogen in a hydrogen-air diffusion flame using two-step saturated fluorescence detection from a series of linear images averaged over twenty laser shots (Ref. 36).

ing in a laminar hydrogen-air diffusion flame are shown in Figs. 7 and 8 respectively. In the case of H-atom imaging, two-step saturated fluorescence was used, requiring two pulsed laser sources with overlapping beams. The first laser, operating at 243 nm, raised atoms to the 2S state by two-photon excitation of the 1S-2S transition, while the second laser, tuned to 656 nm, saturated the 2S-3P transition to populate the 3P state. Subsequent fluorescence was monitored at 656 nm (Balmer- α) radiation using an intensified linear diode array with 1024 elements. Two-dimensional maps of H were assembled from a series of linear images for this steady flame. Close synchronization of the pulsed lasers is required in these two-laser experiments, and there are some difficulties in

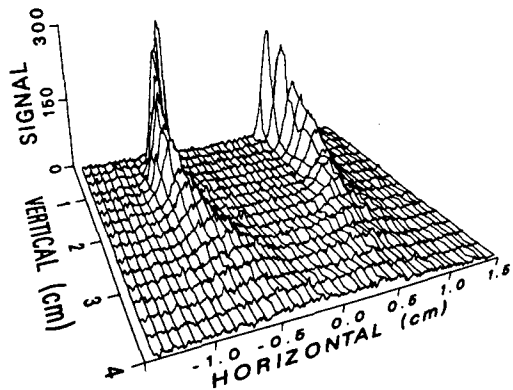
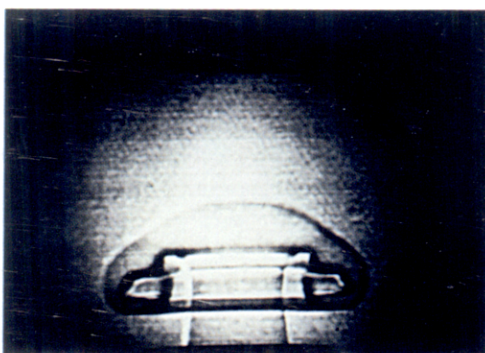
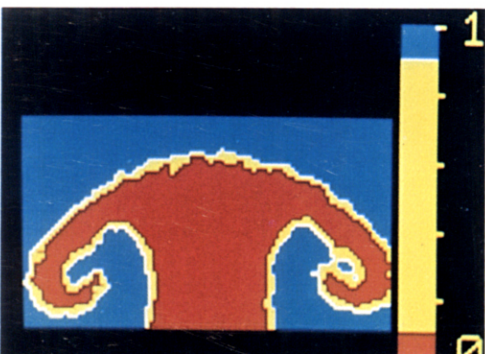


FIG. 8. Mapping of atomic oxygen in a hydrogen-air diffusion flame using two-photon-excited fluorescence detection from a series of linear images averaged over fifty laser shots (Ref. 36).

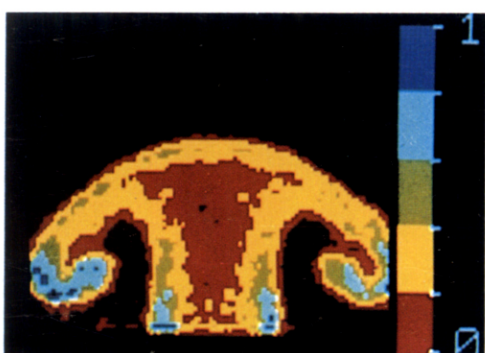
PLANAR IMAGING TECHNIQUES



Laser Schlieren



NO₂ Imaging



OH Imaging

FIG. 2. Comparison of PLIF imaging results with schlieren visualization in a combustion torch (Refs. 18 and 19).

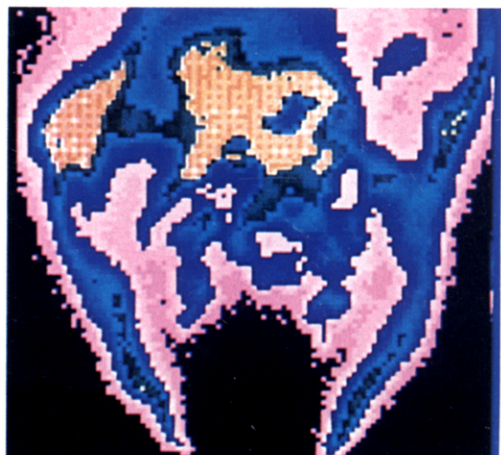


FIG. 4. PLIF image of OH in a spray flame (Ref. 23).

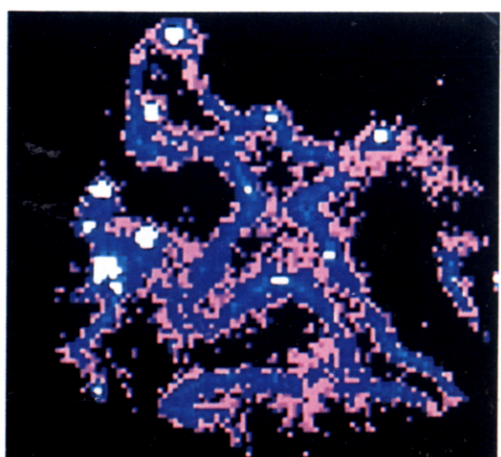


FIG. 5. PLIF image of CH and droplet Mie scattering in a spray flame (Ref. 23).

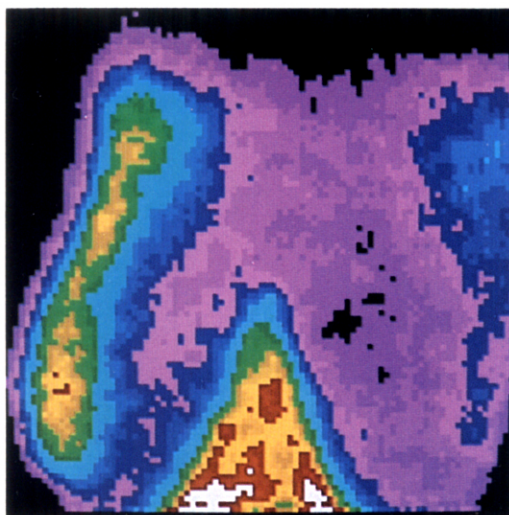


FIG. 6. PLIF image of O_2 in a fuel-rich Meker burner flame. This is a false-color display, with white representing the largest signal and black the smallest (Ref. 32).

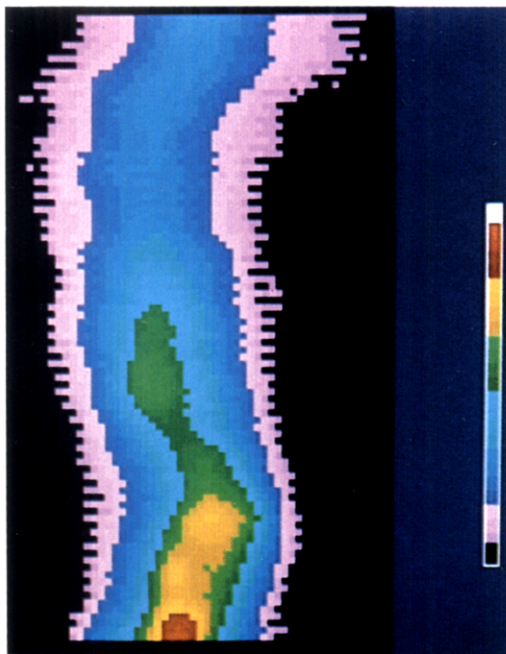


FIG. 9. PLIF image of CO in a CO-air diffusion flame using two photon excitation (Ref. 38).



(a)



(b)



(c)

FIG. 10. Fluorescence imaging in an evaporating spray (Ref. 8). (a), vapor only; (b), liquid only; (c) liquid and vapor.

PLANAR IMAGING TECHNIQUES

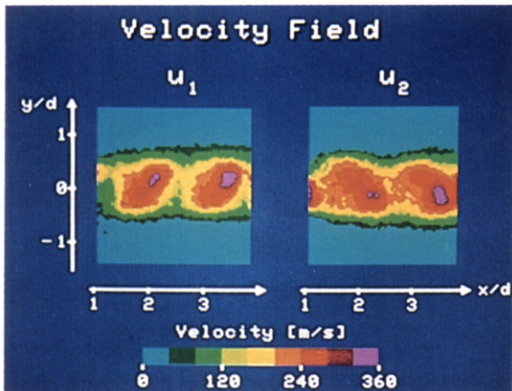


FIG. 14. Velocity imaging (see Fig. 12) in an underexpanded supersonic jet (Ref. 49).

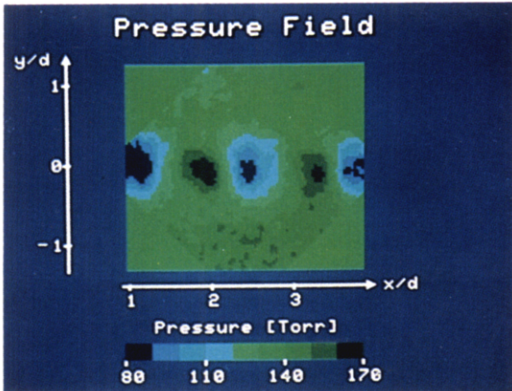


FIG. 15. Pressure imaging in an underexpanded supersonic jet (Ref. 49).

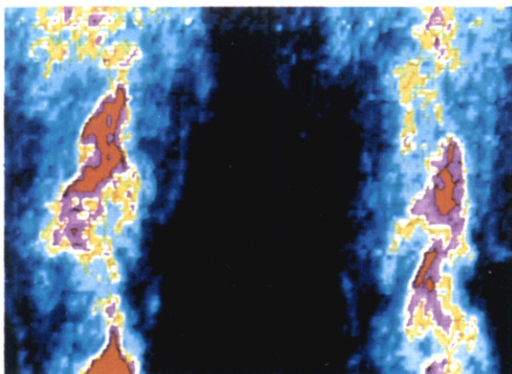


FIG. 16. Two single-shot Raman images of CH_4 in a turbulent nonpremixed $\text{CH}_4\text{-H}_2\text{-air}$ flame (Ref. 46). The region imaged is from 4.9 to 9.9 jet diameters ($d = 1.9$ mm) downstream. Exit velocity = 70 m/sec.

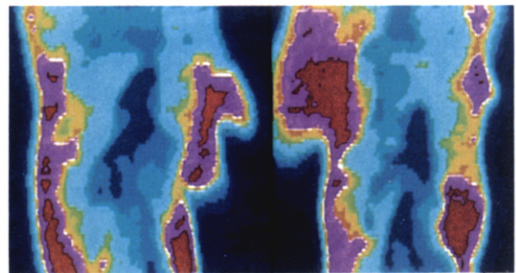


FIG. 17. Single-shot Rayleigh images of temperature in the turbulent flames shown in Fig. 16 above (Ref. 46).

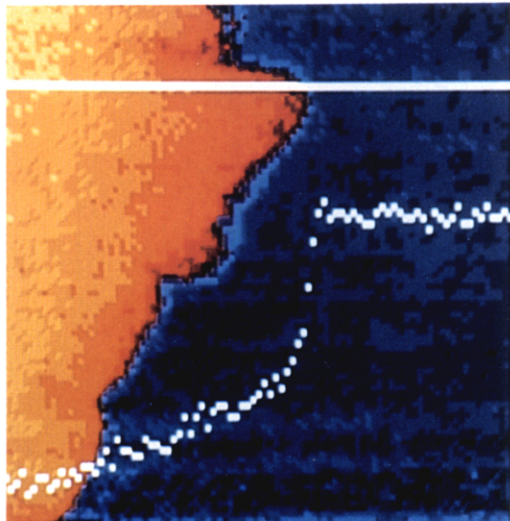
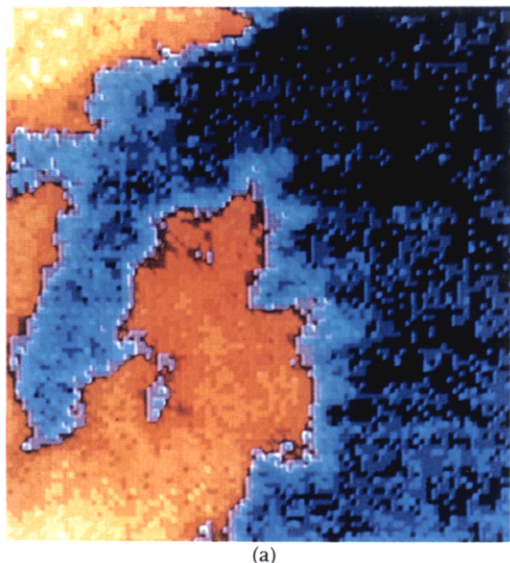


FIG. 20. Mie imaging of flame propagation in a spark-ignition engine (Ref. 71). (a), 1200 rpm; (b), 300 rpm.



FIG. 21. Mie imaging in a propane-air jet flame (Ref. 68).



FIG. 22. PLIF image of unsteady jet obtained with high-resolution (348×576 pixel), high dynamic range CCD camera (Ref. 30).

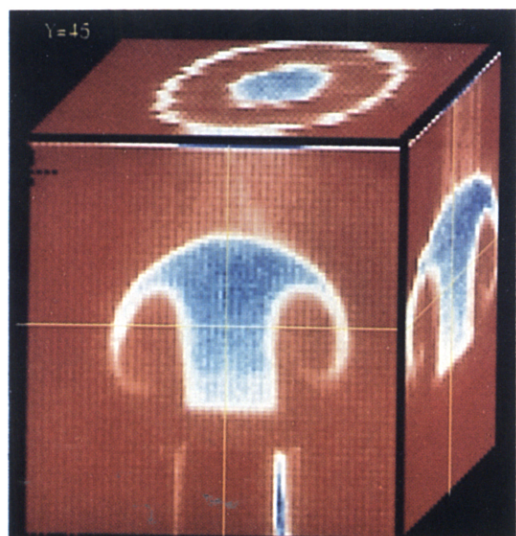


FIG. 23. Display of 3-d image data for a forced jet mixing with co-flowing stream (Ref. 30).

calibrating the measurements, but the results obtained illustrate the potential of this method. The results for O-atoms (see Fig. 8) were obtained in the same flame, though not simultaneously, using two-photon excitation at 226 nm to pump the 2^3P_2 - 3^3P transition of O. Subsequent emission at 778 nm from decay of the 3^3P state (populated by collisional energy transfer from the 3^3P state) down to the 3^3S state was observed (through an interference filter) on the same intensified diode array. The peak O-atom mole fractions, estimated to be in the range between 0.1 and 1%, are found to occur, as expected, in a thin reaction (flame) zone separating the fuel and oxidizer.

The extension of multi-photon LIF imaging of CO is important owing to its significance as a combustion intermediate or product species, as well as its use as a simple fuel in basic experiments. In the imaging experiments reported thus far, a common pumping scheme was employed which involved two-photon excitation (at 230.1 nm) from the $X^1\Sigma^+$ to the $B^1\Sigma^+$ state. Subsequent emission to various vibrational levels of the $A^1\Pi$ state, at wavelengths from 451 to 725 nm, was monitored through an appropriate filter on both 1-d³⁷ and 2-d^{38,39} intensified diode arrays. Sample results³⁸ obtained with single-shot 2-d imaging in the central vertical plane of a CO-air diffusion flame are shown in Fig. 9. The 4 cm × 4 cm region imaged is located just above the exit of the 6 mm dia fuel tube. The laser energy was 2 mJ per pulse at the entrance to the multi-pass cell, which served both to maintain the beam intensity over a large region and to provide a more uniform intensity distribution than obtained in a single-pass configuration. The low-speed flame was unstable, and the resulting low-frequency oscillation in flame position is apparent in this figure. Modelling of the two-photon LIF process, needed to render the imaging quantitative, is still under development,³⁹ but the sensitivity demonstrated in this and other CH₄-air flames suggests that CO imaging will become a useful tool in studies of combustion aerodynamics.

Another variation of multi-photon excitation which is emerging for imaging applications is planar multi-photon dissociation (PMPD), in which multiple photons are used to photolyze an initial species, leaving one of the reaction products in an excited state which subsequently emits fluorescent light. In the one current example of this method,²³ an ArF laser (193 nm) is used to fragment C₂H₂, via a two-photon process, leading to strong CH ($A \rightarrow X$) emission at 431 nm. Imaging this emission serves to mark the location of C₂H₂, and hence the hot unburned fuel regions, in combustion flowfields.

Liquid/Vapor Imaging

In an important extension of gas-phase imaging, it has been shown⁸ that organic exciplexes can be used to enable simultaneous imaging of vapor and liquid distributions present in evaporating sprays. These exciplexes (**excited state complex**) are formed through a reversible reaction involving the parent fuel and an additive organic compound with the effect of shifting the liquid-phase fluorescent emissions by up to 150 nm from the peak of the gas-phase emission.⁴⁰ Thus the fluorescence from both phases can be visualized simultaneously using a single-wavelength laser source. An example of this approach, obtained in a hollow-cone spray of hexadecane doped with naphthalene and tetramethyl-p-phenylene diamine (TMMPD), is shown in Fig. 10 (from Ref. 8). These three fluorescence-imaging results were obtained with multiple laser shots of quadrupled Nd:YAG at 226 nm using separate spectral filters and color film as the recording medium. Work is in progress to incorporate a 2-d diode array camera for recording these images.⁴¹ Although there are difficulties in quantifying this technique and in extending it to combusting flows,⁴² the method is likely to be of considerable use in studies of evaporating sprays relevant to combustion. Finally, it should be noted that the developers of this exciplex approach have hopes of extending the method to yield droplet temperature.⁴³

A related fluorescence-based imaging diagnostic for fuel spray characterization has also been reported.⁴⁴ In this technique, the sprayed liquid is doped with a fluorescent dye and illuminated with a sheet of cw He-Cd laser light (10 mW at 421.6 nm). The resulting fluorescence is imaged at right angles onto an intensified TV camera, and the images are subsequently processed digitally. When the absorption is low, the fluorescent emission is directly proportional to the mass of fuel instantaneously present in the imaged volume. This new diagnostic thus gives direct information on the spray nozzle distribution pattern which is needed in developing improved spray nozzles and models of fundamental spray processes.

Temperature Imaging

Temperature is a critical parameter in many combustion flowfields and so the development of temperature imaging is particularly important. Successful 2-d imaging results have already been reported based on both PLIF^{28,45} and planar Rayleigh scattering,⁴⁶ though the latter is more correctly viewed as a density

measurement. There are two current strategies for LIF-based temperature imaging: two laser (i.e., two-line) excitation schemes in which the ratio of two fluorescence signals is used to infer the relative population in two absorbing levels, and hence the temperature through the Boltzmann relation; and one-laser excitation schemes using either a spectrally narrow or broad laser source and either broadband collection or ratios of narrowband signals.

The two-line scheme has been evaluated⁴⁵ in the postflame region of a premixed flat flame burner using the $Q_1(5)$ lines in the (1,0) and (1,1) vibrational bands of OH ($A \leftarrow X$ system). The broadband fluorescence was detected with an intensified vidicon camera, and the ratio of the LIF signals for the two excitation pulses, corrected for laser pulse energy, was formed at each pixel in the 100×100 array. Since the transitions pumped have a common upper state, the fluorescence yield is the same and the LIF signal ratio depends directly on the relative populations in the vibrational levels $v'' = 1$ and 0, and hence the temperature. Although successful results were obtained, with a stated precision of 10%, the method is limited to regions with a sufficiently high temperature to produce significant populations of OH. Thus an alternative compound such as NO may be preferred. The requirement for two lasers is a serious disadvantage in some cases.

One variation of the single-laser approach which has been demonstrated²⁸ involves use of a stable tracer molecule, such as NO, which can be seeded into the flow at a constant mole fraction X_s . In this case the LIF signal (see Eq. 1) is proportional to a simple function of temperature:

$$S(T) \propto X_s F_{v''}(T) / \sqrt{T}$$

where the specific temperature dependence can be dominated by the Boltzmann fraction in the absorbing state (or states), $F_{v''}$, and only weakly affected by the assumed temperature dependence of the electronic quench rate. An example of single-shot results obtained in a rod-stabilized CH₄-air flame, using an intensified 100×100 photodiode array camera and exciting the $Q_1(22)$ line of NO at 225.6 nm, is shown in Fig. 11.²⁸ The temperature contours are spaced by 200 K, and the asymmetric pattern results from the unstable nature of the flame. The optimum choice of the transition pumped is a function of the desired sensitivity and temperature range of interest. This particular line enabled a self-calibrating procedure.²⁸ The level of NO seeding was about 2000 ppm, and there was no evidence of significant NO reaction occurring in the fuel-lean flows investigated. The estimated ac-

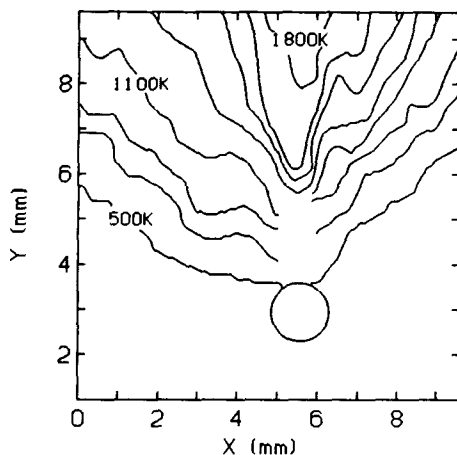


FIG. 11. Temperature imaging in a rod-stabilized methane-air flame using PLIF of NO (Ref. 28).

curacy of these initial measurements was 100–200 K, or about 5–10%, but improvements in the experimental system, including the laser energy, should enable a significant reduction in measurement error. In addition to its primary advantages of requiring only a single laser source and producing an “instantaneous” temperature map, this method is applicable to nonreacting flows.

Velocity and Pressure Imaging

Variations of PLIF also have been developed for imaging 2-d fields of velocity in subsonic^{17,48} and supersonic flows^{9,10,49} and extended to include pressure in one case,⁴⁹ though the applications thus far have been limited to nonreacting flows. The velocity measurements are based on Doppler-shifted absorption of a narrow-linewidth laser source, with the broadband collection of the subsequent fluorescence serving to indicate the relative absorption. This approach is attractive in that it is nonintrusive and avoids the use of particles, though it requires the presence of a suitable tracer species. Work thus far has been carried out in nitrogen flows seeded with trace levels of iodine (I₂) or sodium vapor, which absorb at readily accessible cw laser wavelengths. The method is quite general, however, and work is in progress to enable measurements with more convenient species such as O₂.⁵⁰

The current strategy for imaging velocity makes use of two laser frequencies, fixed at separate locations within an absorption line of the tracer species, and requires four successive PLIF images to infer two velocity components in the plane of illumination. Sketches of the

experimental arrangement and the relationship of the laser frequencies (and directions) to the absorption line profile are shown in Figs. 12 and 13; details are available in Ref. 49. The excitation was carried out using a tunable, single-mode argon ion laser operating at 514.5 nm which is coincident with the overlapping $P(13)/R(15)$ lines of the (43,0) band of the $B \leftarrow X$ system of I_2 . Four overlapping sheets of light were generated and selected sequentially using a chopper. A piezo-driven intra-cavity etalon was employed to rapidly change the laser frequency of the fourth beam by about 750 MHz (9 axial mode spacings). The four successive fluorescence images were recorded on

separate frames of an intensified 100×100 diode array camera, requiring a total measurement time of about 250 milliseconds for the 200 mW power level available in each laser sheet. The size of the region imaged was 16 mm × 16 mm, yielding individual measurement volumes 160 $\mu\text{m} \times 160 \mu\text{m} \times 80 \mu\text{m}$. The measured signals were corrected for beam intensity variations and then input to simple relations⁴⁹ to infer the velocity components. An important advantage of the two-frequency scheme is that it is self-calibrating and requires no prior knowledge of the line-shape function. Further, the measurements also yield the slope of the line which may be used to infer pressure when pressure broadening is sufficiently large.

Example images obtained in an underexpanded Mach 1.5 supersonic jet, with a background pressure of 125 Torr, are shown in Figs. 14 and 15 for velocity (two components) and pressure respectively.⁴⁹ The results successfully replicate the major features expected within the shock cells imaged. The appearance of the images is compromised by the need to display only a modest number of color scales for clarity, though the data are actually recorded to 8-bit resolution. The estimated error in the velocity measurement is 8% (at the maximum velocities) and is about 15% for pressure, but improved accuracy as well as temporal resolution may be expected in future work. Additionally, it may be possible to incorporate simultaneous determinations of temperature and density.

Although PLIF imaging of velocity is still in an early stage of development, with significant challenges yet to be resolved, the potential of the method is clear. If sufficient improvements can be made, then the velocity data can be used in novel ways, for example to calculate "images" of various velocity correlations or the vorticity distribution and their evolution. When considering fluorescence-based approaches, however, one should be aware of the progress being made with competitive imaging techniques, such as those based on particle-tracking or laser-marking concepts. As an example, stereoscopic visualization using scattered light from tracer particles in liquid flows has recently been coupled with advanced digital image processing to yield 3-d velocity information at a much improved rate.⁵¹ Visualization based on laser-induced phosphorescence,⁵² Mie scattering from laser-induced aerosols (laser "snow"),⁵³ and even Raman excitation with subsequent LIF tracking⁵⁴ are other possibilities for extracting velocity field information, though these methods currently appear to have less potential than LIF for high-speed and low-density flows.

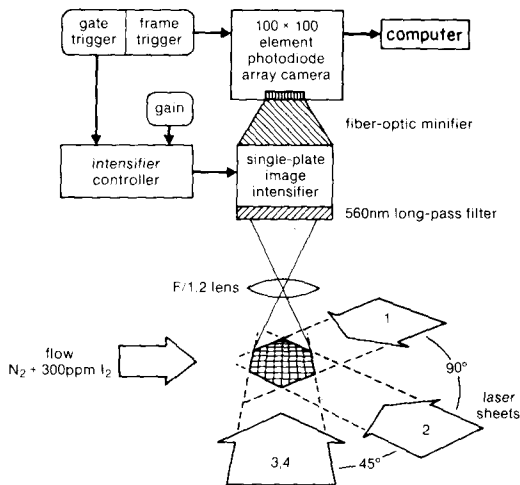


FIG. 12. Illumination scheme and apparatus for PLIF velocity imaging (Ref. 49).

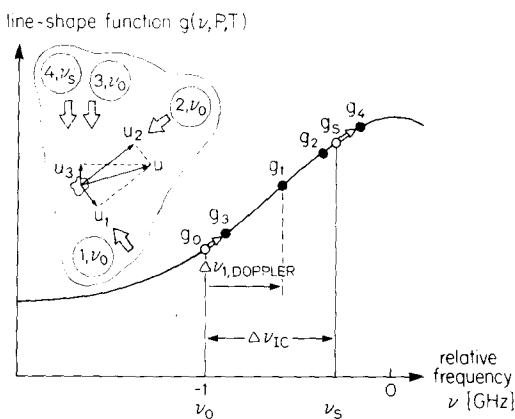


FIG. 13. Relative frequencies with four-beam velocity-pressure imaging scheme (Ref. 49).

Spontaneous Raman Imaging

Species-specific imaging can also be carried out using spontaneous Raman scattering, though the applicable cross-sections are many orders-of-magnitude smaller than for LIF. The initial use of this method for planar imaging was reported in 1973 by Hartley, who coined the name Ramanography.⁵⁵ His early work was performed with nonreacting gases at high pressures, in order to produce measurable signal levels, and made use of photographic recording of intensified images. Ten years of progress in laser and detector technology were required before the first single-shot 2-d Raman imaging was performed in flame gases.⁷ The experiments, of a turbulent diffusion flame, were conducted with D_2 as the fuel to provide a relatively large scattering cross-section, but the weakness of the process still required the use of a multi-pass cell and a unique high-energy (1.5 J), long-pulse (1.8 μ sec) dye laser (500 nm).

Spontaneous Raman scattering has received considerable attention as a combustion diagnostic, primarily for single-point measurements (see Ref. 56 for an overview) of major species and temperature. Thus the physics aspects, involving inelastic scattering between incident photons of light and the internal energy modes of the molecules, usually the vibrations, are well understood. Raman diagnostics are attractive because no tunable laser is required and, in principle, several species can be probed simultaneously. Unfortunately, the weakness of the process generally limits its application to clean flames (free of interference from Mie scattering) with low luminosity, and to measurements involving major species.

An example of current capability of single-shot Ramanography in flames is shown in Fig. 16.⁴⁶ The experiments were carried out in turbulent, nonpremixed CH_4-H_2 -air (38% CH_4 , 62% H_2) flames at atmospheric pressure, and the species imaged was CH_4 , which has a large Raman cross-section (about 9 times that of N_2). The laser provided about 200 mJ of energy at 440 nm in a 1.8 μ sec pulse, and a multi-pass cell was used to increase the intensity by a factor of about 30 over that present in a single pass. The scattered light from the sheet was collected and split into two parts to enable simultaneous detection of Raman and Rayleigh scattering (the latter being used to measure temperature as discussed in the following section). The Raman-scattered light was filtered spectrally and imaged onto a gated, intensified vidicon camera. The region imaged was 1.2 cm \times 1.0 cm, located on the jet centerline from 4.9 to 9.9 diameters ($d = 1.9$ mm) downstream, and was

digitized in an 80 \times 70 format. The interpretation of the Raman signal is straightforward because, for full collection of the Q-branch, the signal is essentially directly proportional to the concentration. In these experiments the method was self-calibrating in that the peak concentrations are known from the monitored inlet conditions. The signal detection limit was about one-tenth of the maximum signal observed.

The results obtained thus far with Raman imaging are promising, in terms of the method being useful for studies of large-scale flowfield structures under selected conditions, but the weakness of the process suggests that measurements will be limited to major species. The combined use of Raman imaging with another planar diagnostic,^{46,57} such as Rayleigh scattering or PLIF, enabling simultaneous mapping of two scalar quantities, should be valuable in studying reaction flowfields.

Rayleigh Imaging

Laser Rayleigh scattering is a well-developed diagnostic tool that is useful in both cold and hot reacting flows.⁵⁸ Although employed primarily for single-point recording, this method has considerable potential for multiple-point measurements owing to the favorable magnitude of the scattering cross-section which is much larger than for Raman scattering but smaller than for LIF. Results have been reported for: 1-d imaging of temperature in diffusion flames,^{58,59} 2-d imaging of gas concentration in a cold jet³ and temperature in a turbulent nonpremixed flame;⁶⁰ two-plane 2-d imaging of gas concentration in a cold jet enabling determination of the 3-d gradient of the scalar;⁶¹ and even 3-d imaging of gas concentration, achieved by recording multiple planes of 2-d images in a photoacoustically perturbed jet.⁶²

The physical process in Rayleigh scattering is elastic in nature, that is it results in light unshifted in wavelength from the illumination beam. Consequently there is no way to distinguish the scattering between the various gaseous constituents, or indeed from other elastic scatterers such as particles or surfaces present in the beam path. Since particle scattering has very large cross-sections, the flow under study must be extremely clean, and this generally limits application of Rayleigh scattering to controlled laboratory environments. The Rayleigh-scattering cross-section is a function of the refractive index of each species⁶³

$$\sigma_{R_i} = (4\pi^2/\lambda^4) [(n_i^2 - 1)/N]^2$$

where λ is the incident wavelength, n_i the refractive index of the species i , and N the molecular number density at STP. Thus species specificity is generally possible only in simple flows where, for example, a gas with a high refractive index, such as freon, discharges into a gas of low index, such as helium. Equally common is to choose mixtures with a nearly constant mass-normalized total cross-section, so that the Rayleigh signal is proportional to the mass density of the gaseous mixture. Similarly, a constant mole-fraction-weighted cross-section can be employed so that, for constant pressure, scattering measurements may be used to infer temperature.⁶⁰ Although this approach imposes strict constraints on mixtures studied and is subject to errors when the mixture is reactive, the simplicity and economy of the diagnostic are attractive for imaging density and temperature.

Examples of Rayleigh-imaging thermometry results for a turbulent nonpremixed CH₄-H₂-air flame are shown in Fig. 17.⁴⁶ These images were acquired simultaneously with the Raman-based CH₄ concentration data displayed in Fig. 16, and hence the results in these two figures should be compared directly. The fuel-gas composition was selected so that its Rayleigh scattering cross-section was the same (within 2%) as that of the ambient air and the combustion products. As described in the previous section, the laser source operated at 440 nm and produced 200 mJ per pulse. This short wavelength aids the Rayleigh signal considerably owing to its $1/\lambda^4$ dependence. The temperature values obtained were in the range from 300 to 2000 K, with different temperature ranges displayed by different colors. The simultaneous temperature and CH₄ images are of course closely related, with the concentration result appearing nearly as the negative of the temperature image. This follows from the simple fact that the concentration varies inversely with temperature, and that the regions of greatest spatial gradient in temperature must also be the regions of greatest gradient in fuel fraction.

A schematic of the arrangement used in Rayleigh imaging the instantaneous concentration field of freon discharging into co-flowing nitrogen is shown in Fig. 18.³ Sample results are shown in Fig. 19. The laser source was a pulsed Nd:YAG system ($\lambda = 532$ nm) providing 20 mJ in a 15 nsec pulse, which yielded acceptable single-shot signal levels to visualize large-scale features of the flow. This study included a comparison of Mie and Rayleigh scattering techniques for studies of jet mixing. The primary conclusions were that Rayleigh imaging provides finer spatial resolution and hence

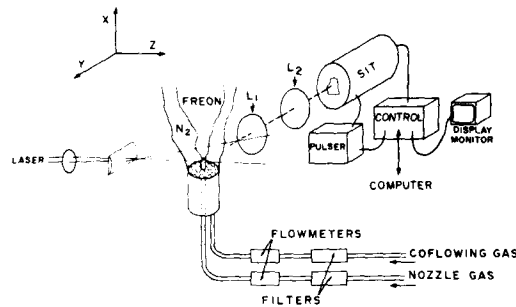


FIG. 18. Experimental arrangement for Rayleigh imaging (Ref. 3).

a significant improvement in terms of detecting molecular diffusion effects. Mie scattering of course leads to much higher signal levels, so that it is necessary to employ significantly higher laser intensities with Rayleigh imaging.

Mie Imaging

The use of scattered light from small particles, known generally as Mie scattering, is attractive for flow visualization owing to the large strength of the process relative to the

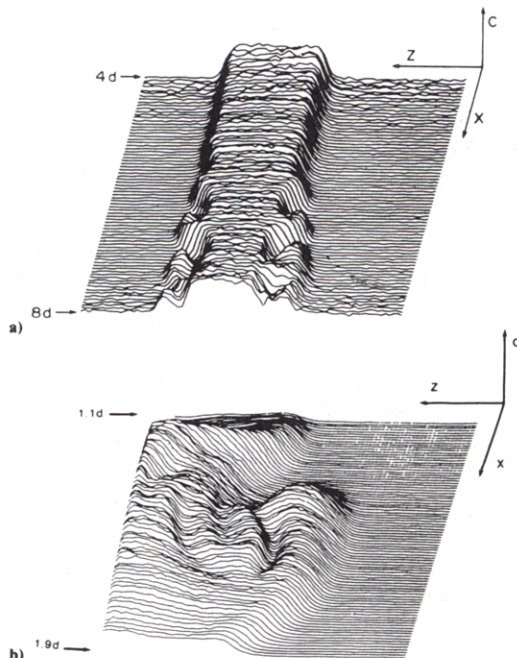


FIG. 19. Instantaneous concentration profiles of a coflowing turbulent jet (freon into nitrogen) obtained by Rayleigh scattering. a) The jet from 4d to 8d; b) A smaller region of the jet (Ref. 3).

other scattering mechanisms considered in this paper and to the fact that fixed-frequency laser sources may be employed. Thus Mie scattering, using a relatively simple laser source and either film or an unintensified array camera as the recording medium, provides a convenient, economical method for planar flowfield imaging. The primary disadvantages of Mie scattering are that there may be slip between the motion of particles and the surrounding gas and that the process does not directly sample the gaseous composition. Slip can be minimized through use of sufficiently small particles, though at the expense of the scattering cross-section. The lack of species specificity has in the past generally limited planar Mie imaging to studies of mixing between seeded and unseeded streams, mostly involving nonreactive flows^{2,64,65} though some results have been reported in flame systems.^{66,67} A recent significant advance, however, has been to employ gaseous seed material which produces light-scattering particulates at a reactive interface, thus providing an enhanced degree of chemical information.^{68,69}

The underlying physics of Mie scattering, relevant to the prediction of imaging signals for specified illumination, particle properties and number density, is well established.⁷⁰ In general, the high scattering cross-section allows use of either pulsed or cw laser sources, and a sheet of illumination, typically less than 1 mm in thickness, is formed with simple spherical and cylindrical lenses. The scattered light is collected at right angles and focussed onto either film or an unintensified array camera. Film of course offers higher spatial resolution, and can be conveniently used for high-repetition-rate recording, but solid-state cameras offer essentially real-time display capability and have advantages when quantitative interpretation of signal levels is important.

An impressive example of planar Mie imaging in a challenging combustion environment is provided by a recent study of flame structure in an operating internal combustion engine.^{67,71} In brief, a thin sheet of laser light, generated with 200 mJ from a single 10 nsec pulse from a frequency-doubled Nd:YAG laser, was propagated across the engine cylinder parallel to the top surface of the piston. The intake flow (propane plus air, in stoichiometric proportions) was seeded with sub-micron TiO₂ particles, and the images of Mie scattered light were obtained at right angles through a transparent cylinder head and recorded on an unintensified 100×100 diode array camera. Since the number density of particles is coupled to the gas density, the images may be viewed as an

instantaneous map of gas density. The laser was pulsed when the turbulent flame front was near the center of the combustion chamber, about 9 degrees before TDC and about 6 degrees after firing the spark. The spark plug was mounted in the piston top (about 2.2 cm from the center of the 8.3 cm int. dia cylinder) to enable unrestricted imaging. The data were digitized to high resolution, and are displayed in false color using a 16-color scale. Example results obtained at engine speeds of 300 and 1200 rpm, for a 1 cm × 1 cm field of view located at the center of the cylinder, are shown in Fig. 20.⁷¹ The blue and black areas represent high scattering intensity and therefore the low temperature, high density zones of unburned gases, while the yellow region contains the low density, high temperature burned gases.

In order to quantify the flame thickness, the intensity data were plotted quantitatively along specified lines or rows of pixels (see Fig. 20). From analysis of such data, it was determined that the flame fronts were quite thin, on the order of 100 microns, and mostly continuous. Another primary observation was that as the turbulence intensity was increased, by raising the engine speed, the flame front changed from a gently wrinkled, laminar character to a more convoluted and less continuous form, with increasing frequency of pockets of unburned gases.

Recently, Mie imaging has been extended to enable visualization of reactive interfaces in flowfields with mixing.^{68,69,72} This is a useful development, already adopted by several groups in a short time, in that the method retains the signal level advantages of Mie scattering while adding a degree of chemical sensitivity not present in Mie imaging of flows seeded with preformed particles. The most common variation of this approach involves the use of TiCl₄ vapor, seeded into a gaseous stream free of water vapor. At the interface of this flow with a separate stream containing water vapor, or at the location that water vapor is produced as a result of combustion of dry air and fuel, submicron-sized particles of TiO₂ are rapidly formed, and the light scattered from these particles can be used to image the region where the TiCl₄ first meets water vapor. Example results obtained with this method applied to a study of jet flames are shown in Fig. 21 (from Ref. 68). In this case the light sheet was provided by a single pulse of frequency-doubled Nd:YAG laser light, and the green Mie-scattered light was collected at right angles and focused onto film as the recording medium. Also recorded was the orange-colored luminosity of soot in the flowfield, which provides complementary information on flame

front location. The propane fuel exited through a 10 mm dia nozzle with an initial velocity of 1.2 m/sec ($Re = 2700$), and subsequently mixed and burned with low velocity co-flowing dry air. Both streams were seeded with $TiCl_4$ so that the resulting TiO_2 particles mark both the cool air/ H_2O interface outside the flame and the cool fuel/ H_2O interface inside the flame. This imaging scheme clearly reveals details of the flowfield structure that were not apparent in schlieren and shadowgraph visualization data acquired in the same study.⁶⁸

There are other possibilities for utilizing Mie scattering to image selected regions of flows. As an example, recent work has shown that measurable levels of soot are formed at or very near the flame front in methane-air diffusion flames. Since this soot does not appear to persist beyond the flame zone, images of scattered light from such soot can be used to map the instantaneous flame position. Although 1-d imaging was employed in the one study reported thus far,⁶⁹ using a cw argon-ion laser source and an unintensified linear photodiode array, the method should be readily extended to planar imaging.

Trends in Planar Imaging

Planar imaging techniques have advanced rapidly, to a stage that selected methods are now used as tools in studies with a combustion aerodynamics focus. Further developments in imaging diagnostics can be projected based on current research, though the field is new enough to leave room for creative surprises.

Imaging diagnostics developments are driven by combustion measurement needs, which are relatively fixed, and at the same time are constrained by the fast-evolving capabilities of laser sources and solid-state cameras. This situation enables prediction of some trends with high confidence, for example the recording of planar images with increased repetition rates and spatial resolution (more pixels per camera frame). These improvements will enable detailed study of small- and large-scale flowfield features and their temporal evolution. Steady progress can also be anticipated in extending the list of species accessible by PLIF imaging, not only by single photon excitation but also through the use of multi-photon and photo-fragmentation schemes. In this connection, current work on fluorescence imaging of O_2 is of special importance owing both to the significance of this species and to its potential in imaging temperature⁷³ and velocity.⁵⁰ With expected simplifications in imaging apparatus,

experiments involving simultaneous imaging of multiple quantities, for example imaging multiple species or temperature together with species, will become more common. With improved availability of tunable, narrow-linewidth laser sources, both cw and pulsed, variations in PLIF imaging based on absorption lineshape concepts may be expected. In contrast, use of spectrally broad sources offers prospects for instantaneous particle sizing by quantitative planar imaging of Mie-scattered light.⁷⁴

On a more speculative level, if velocity imaging schemes can be improved sufficiently, it should be possible to convert such images to maps of vorticity (and the evolution of vorticity), or to correlate velocity/vorticity with other imaged properties. Similarly, refinements in species and temperature data will allow image processing on a higher level, enabling determination of scalar gradients and various spatial and temporal correlations. And, in time, these parameters will be measured using full 3-d data sets.

The impact of planar imaging on combustion and fluid mechanics modelling is not yet clear, though the futures of imaging diagnostics and advanced modelling are surely intertwined and it is likely that the changed nature of data available through imaging will lead to changes in modelling perspectives and methods.

The area of camera technology is central to imaging, and impressive advances are being made in the performance and convenience of solid-state detector array systems. The trend toward high-resolution, low-noise CCD arrays is particularly notable, with large, 1000×1000 pixel arrays now available commercially. These arrays have architecture which will enable very flexible use of pixels. For example, it is now possible to use a large array as a piece of "electronic film," that is to record several separate images on a reduced area of the array and to transfer the image data electronically on the chip for short-term storage. In this way the array can be used as a high-speed digital camera. Alternatively, many images may be recorded on the array, at separate locations, so that the array functions as an "electronic plate" on which many separate images have been recorded, as with a rotating prism camera.²⁰

Research with high-resolution image sensors is already in progress in the combustion imaging community. An early example of such work is illustrated in Fig. 22 which is a PLIF image of an unsteady, room temperature nitrogen jet issuing from a 5 mm dia nozzle at an initial velocity of about 10 cm/sec.³⁰ The flow has been seeded with biacetyl to enable fluorescence imaging at visible wavelengths; in this case the

light source was a pulsed xenon fluoride (XeF) laser, at 351 nm, and the emission is broadband but appears green to the eye. The solid-state camera was a commercial unit with a Thomson-CSF 576×384 CCD array. This sensor is operated at reduced temperature (-125°C) to reduce dark current and the circuitry is specially designed for low-noise performance; the resulting measured background noise level is about 10 photoelectrons per pixel. The key performance advantages of this array, relative to currently common 100×100 and 128×128 photodiode arrays, are: a higher fill factor for the active portion of the imaging sensor (93%), which leads to more efficient use of light; a high quantum well depth, about 5×10^5 photoelectrons, which together with the low noise level provides for greater than 4 decades of linear dynamic range (defined as the ratio of the largest detectable signal to the signal level where the signal-to-noise ratio is 1:1); a much larger number of pixels, which will allow observation of a greater range of scale sizes in a single image and also will enable development of electronic-film schemes for recording multiple images between read-out cycles; and finally, the use of a cooled CCD eliminates the need for a complex image intensifier, when the scattered light is in the sensitive region of the array. This new camera is still undergoing evaluation,^{17,30} but its superior dynamic range and spatial resolution are already apparent. For example, in Fig. 22 the intensity has been divided into 9 major ranges (corresponding to the dark contours in the figure), and each range has been further subdivided into 6 color levels. Thus more than 50 distinct levels are apparent when the data are displayed on a high-resolution color monitor. Unfortunately that level of resolution is difficult to convey on a small print such as Fig. 22. Controlled tests of the system have verified that 12-bit resolution of the signal is possible, in contrast with the 6-7 bit capability of cameras in current use.

Another important trend in flow imaging research is to establish the capability for 3-d imaging, for example by simply scanning the recording plane employed in 2-d imaging. Initial results based on this approach are now available for both Rayleigh⁶¹ and fluorescence⁷⁵ imaging. The effort in this area of imaging research is presently directed toward two main issues: the need to record multiple planes of image data in a short time, so that the data approach the instantaneous 3-d distribution; and questions of how to display and to use 3-d data. The former issue is being addressed with both a short-term and a longer-term strategy. In the short term, recording rates of up to

about 500 Hz will be employed, as both laser sources (e.g., excimer-pumped lasers) and solid-state cameras (e.g., photodiode array systems) are available with such capability. The long-term strategy is less clear and may involve, on the laser side, use of either metal vapor laser systems capable of operation up to about 20 kHz, laser systems based on amplification of a high-repetition-rate train of short pulses from a mode-locked laser source, or possibly a long-pulse laser of duration suitable for recording multiple frames in one laser shot. On the recording side, the most promising schemes seem to be those mentioned above based on electronic-film and -plate concepts. The latter presents some difficult challenges but should enable imaging into the MHz regime.

As to the question of display of 3-d image data, there are several possibilities suggested by the state-of-the-art in fields where image data are already in use. There are, however, important differences between imaging solid objects with distinct boundaries and imaging flow properties which have more diffuse distributions, and these differences complicate predictions of the future. It may be that the value of 3-d data is less likely to accrue, in the long term, from the visual use of 3-d data displays than from the need for 3-d data to infer quantities, such as property gradients and spatial correlations, which have an inherent 3-d rather than a 2-d character. Nonetheless, there is a need for 3-d displays of flowfield properties for at least qualitative use in studying flowfields, and the future will surely lead to exciting developments in this area of research.

As an example of current capability of 3-d display of PLIF data, Fig. 23 shows three slices or cuts through the flowfield of an axially forced jet mixing with a surrounding slow-flowing stream.⁷⁵ The nitrogen jet was seeded with biacetyl to enable fluorescence imaging, and the 3-d data set was compiled by sequentially recording 24 individual vertically-oriented planes of data spaced across the width of the jet. Although each plane of data (100×100 pixels) was recorded with a single laser pulse, thus freezing the flow, the 24 planes were recorded in separate cycles of the highly reproducible, cyclic flow. The locations of the three planes shown in this single-frame display are set by movable cursors (see the lines visible on the sides of the display "box"), and the display program allows wide flexibility both in the orientation of the planes displayed and in the rate of change of the display, so that the planes may be scanned with time to provide a "3-d movie". The quantity of information stored in such single data sets (2.4×10^5 pixels with the

100×100 pixel camera, and nearly 6 megapixels with the 576×384 pixel camera!) serves as an impressive indicator of the potential of planar and 3-d imaging.

Acknowledgements

The author is pleased to acknowledge the important contributions made to Stanford's imaging diagnostics program by several colleagues and graduate students, particularly G. Kychakoff, R. Howe, P. Paul, M. Allen, B. Hiller, J. Seitzman, M. Lee and J. McDaniel. Our research has been sponsored by the Air Force Office of Scientific Research; we are grateful for this support and for the advice and encouragement provided by our technical monitors, Len Caveny and Julian Tishkoff.

REFERENCES

1. ECKBRETH, A. C.: *Eighteenth Symposium (International) on Combustion*, p. 1471, The Combustion Institute, 1981.
2. LONG, M. B., WEBBER, B. F. AND CHANG, R. K.: *Appl. Phys. Lett.* 34, 22 (1979).
3. ESCODA, M. C. AND LONG, M. B.: *AIAA J.* 21, 81 (1983).
4. ALDÉN, M., EDNER, H., HOLMSTED, G., SVANBERG, S. AND HOGBERG, T.: *Appl. Opt.* 21, 1236 (1982).
5. DYER, M. J. AND CROSLEY, D. R.: *Opt. Lett.* 7, 382 (1982).
6. KYCHAKOFF, G., HOWE, R. D., HANSON, R. K. AND McDANIEL, J. C.: *Appl. Opt.* 21, 3225 (1982).
7. LONG, M. B., FOURGETTE, D. C., ESCODA, M. C. AND LAYNE, C. B.: *Opt. Lett.* 8, 244 (1983).
8. MELTON, L. A. AND VERDIECK, J. F.: *Combust. Sci. and Tech.* 42, 217 (1985).
9. CHENG, S., ZIMMERMANN, M. AND MILES, R. B.: *Appl. Phys. Lett.* 43, 143 (1983).
10. McDANIEL, J. C., HILLER, B. AND HANSON, R. K.: *Opt. Lett.* 8, 51 (1983).
11. LUCHT, R. P.: *Laser Spectroscopy and its Applications*, p. 623, Marcel Dekker, 1986.
12. BECHTEL, J. H., DASCH, C. J. AND TEETS, R. E.: *Laser Applications*, p. 129, Academic Press, 1984.
13. CROSLEY, D. R.: *High Temperature Materials and Processes* 7, 41 (1986).
14. KYCHAKOFF, G., HOWE, R. D. AND HANSON, R. K.: *Appl. Opt.* 23, 704 (1984).
15. KYCHAKOFF, G., HANSON, R. K. AND HOWE, R. D.: *Twentieth Symposium (International) on Combustion*, p. 1265, The Combustion Institute, 1985.
16. CATTOLICA, R. J. AND VOSEN, S. R.: *Twentieth Symposium (International) on Combustion*, p. 1273, The Combustion Institute, 1985.
17. KYCHAKOFF, G. AND HANSON, R. K.: Proc. of Int. Conf. on Computerized Multidimensional Imaging and Processing, Irvine, CA, 1986. See also Ref. 30.
18. CATTOLICA, R. J. AND VOSEN, S. R.: *Comb. Sci. Tech.* 48, 77 (1986).
19. CATTOLICA, R. J.: *Twenty-First Symposium (International) on Combustion*, p. , The Combustion Institute, 1987.
20. PAUL, P. H., KYCHAKOFF, G. AND HANSON, R. K.: Stanford University, work in progress, 1986.
21. DYER, M. J. AND CROSLEY, D. R.: *Fluorescence Imaging for Flame Chemistry*, p. 211, Proc. Int. Conf. on Lasers '84, 1985.
22. ALLEN, M. G. AND HANSON, R. K.: *Opt. Engring* 25, 1309 (1986).
23. ALLEN, M. G. AND HANSON, R. K.: *Twenty-First Symposium (International) on Combustion*, p. , The Combustion Institute, 1987.
24. ALLEN, M. G., HOWE, R. D. AND HANSON, R. K.: *Opt. Lett.* 11, 126 (1986).
25. ALDÉN, M., EDNER, H. AND SVANBERG, S.: *Appl. Phys. B* 29, 93 (1982).
26. ALLEN, M. G. AND HANSON, R. K.: presented at Int. Laser Science Conf., Seattle, Oct. 1986.
27. KYCHAKOFF, G., KNAPP, K., HOWE, R. D. AND HANSON, R. K.: *AIAA J.* 22, 153 (1984).
28. SEITZMAN, J. M., KYCHAKOFF, G. AND HANSON, R. K.: *Opt. Lett.* 10, 439 (1985).
29. ITOH, F., KYCHAKOFF, G. AND HANSON, R. K.: *J. Vac. Sci. Technol. B* 3(6), 1600 (1985).
30. KYCHAKOFF, G., PAUL, P. H., VAN CRUYNINGEN, I. AND HANSON, R. K.: in preparation, 1986.
31. MASSEY, G. A. AND LEMON, C. J.: *IEEE J. Quant. Elec. QE-20*, 454 (1984).
32. LEE, M. P., PAUL, P. H. AND HANSON, R. K.: *Opt. Lett.* 11, 7 (1986).
33. GOLDSMITH, J. E. M. AND ANDERSON, R. J. M.: *Opt. Lett.* 11, 67 (1986).
34. LEE, M. P. AND HANSON, R. K.: *J. Quant. Spectrosc. and Radiat. Trans.* 36, 425 (1986).
35. ALDÉN, M., HERTZ, H. M., SVANBERG, S. AND WALLIN, S.: *Appl. Opt.* 23, 3255 (1984).
36. GOLDSMITH, J. E. M. AND ANDERSON, R. J. M.: *Appl. Opt.* 24, 607 (1985).
37. ALDÉN, M., WALLIN, S. AND WENDT, W.: *Appl. Phys. B* 33, 205 (1984).
38. HAUMANN, J., SEITZMAN, J. M. AND HANSON, R. K.: *Opt. Lett.* 11, 776 (1986).
39. SEITZMAN, J. M., HAUMANN, J. AND HANSON, R. K.: submitted to *Appl. Opt.*
40. MELTON, L. A.: *Appl. Opt.* 22, 2224 (1983).
41. DOBBS, G.: United Technologies Research Center, private communication (1986).
42. MELTON, L. A. AND VERDIECK, J. F.: *Twentieth Symposium (International) on Combustion*, p. 1283, The Combustion Institute, 1985.
43. MURRAY, A. M. AND MELTON, L. A.: *Appl. Opt.* 24, 2783 (1985).
44. BROWN, G. M. AND KENT, J. C.: *Flow Visualization III* (W. J. Yang, Ed.), p. 118, Hemisphere Pub. Corp., 1985.
45. CATTOLICA, R. J. AND STEPHENSON, D. A.: *Dynam-*

- ics of Flames and Reactive Systems, Vol. 95, p. 714, of Progress in Astronautics and Aeronautics, 1985.
46. LONG, M. B., LEVIN, P. S. AND FOURGUETTE, D. C.: Opt. Lett. 10, 267 (1985).
 47. HILLER, B., McDANIEL, J. C., REA, E. C., JR., AND HANSON, R. K.: Opt. Lett. 8, 474 (1983).
 48. HILLER, B. AND HANSON, R. K.: Opt. Lett. 10, 206 (1985).
 49. HILLER, B., COHEN, L. M. AND HANSON, R. K.: AIAA reprint 86-0161, 24th Aerospace Sciences Meeting, Reno, Jan. 1986.
 50. COHEN, L. M., LEE, M. P. AND HANSON, R. K.: Stanford Univ., unpublished results, 1986.
 51. CHANG, T. P., WILCOX, N. A. AND TATTERSON, G. B.: Opt. Eng. 23(3), 283 (1984).
 52. HILLER, B., BOOMAN, R. A., HASSA, C. AND HANSON, R. K.: Rev. Sci. Instrum. 55(12), 1964 (1984).
 53. HASSA, C. AND HANSON, R. K.: Rev. Sci. Intrum. 56(4), 557 (1985).
 54. MILES, R. B.: Princeton University, private communication (1986).
 55. HARTLEY, D. L.: *Laser Raman Gas Diagnostics* (M. Lapp and C. M. Penney, Eds.), p. 311, Plenum, 1974.
 56. ECKBRETH, A. C.: AIAA reprint 86-0138, 24th Aerospace Sciences Meeting, Reno, Jan. 1986.
 57. NAMAZIAN, M., KELLY, J., SCHEFER, R. W., JOHNSTON, S. C. AND LONG, M. B.: Proc. Int. Gas Research Conf., Toronto, 1986. In press.
 58. SMITH, J. R.: Rayleigh Temperature Profiles in a Hydrogen Diffusion Flame, p. 84, Proceeding of the SPIE, Vol. 158, Bellingham, WA, 1978.
 59. DIBBLE, R. W. and Hollenbach, R. E.: *Eighteenth Symposium (International) on Combustion*, p. 1489, The Combustion Institute, 1981.
 60. FOURGUETTE, D. C., ZURN, R. M. AND LONG, M. B.: Comb. Sci. and Tech. 44, 307 (1985).
 61. YIP, B. AND LONG, M. B.: Opt. Lett. 11, 64 (1986).
 62. YIP, B., FOURGUETTE, D. C. AND LONG, M. B.: Appl. Opt. 25, 3919 (1986).
 63. PENNEY, C. M.: J. Opt. Soc. Amer. 59, 34, 1969.
 64. LONG, M. B., CHU, B. T. and CHANG, R. K.: AIAA J. 19, 1151 (1981).
 65. LONG, M. B. AND CHU, B. T.: AIAA J. 19, 1158 (1981).
 66. LYSAGHT, A. J. R., BILGER, R. W. AND KENT, J. H.: Comb. and Flame 46, 105 (1982).
 67. ZUR LOYE, A. O., BRACCO, F. V. AND SANTAVICCA, D. A.: Preliminary Study of Flame Structure in an Internal Combustion Engine Using 2-D Flow Visualization, p. 249, Proc. of the International Symposium on Diagnostics and Modeling of Combustion in Reciprocating Engines, 1985.
 68. CHEN, L.-D. AND ROQUEMORE, W. M.: Comb. and Flame 66, 81 (1986).
 69. MIAKE-LYE, R. C. AND TONER, S. J.: Comb. and Flame 67, 9 (1987).
 70. BOHREN, C. F. AND HUFFMAN, D. R.: *Absorption and Scattering of Light by Small Particles*, Wiley, 1983.
 71. ZUR LOYE, A. O. AND BRACCO, F. V.: Princeton Univ., unpublished results, 1986.
 72. ROQUEMORE, W. M., TANKIN, R. S., CHIU, H. H. AND LOTTES, S. A.: Expts. in Fluids 4, 205 (1986).
 73. LEE, M. P., PAUL, P. H. AND HANSON, R. K.: Opt. Lett., 12, 75 (1987).
 74. ALLEN, M. G. AND HANSON, R. K.: Digital Imaging in Spray Flames, Western States Section paper 85-13, U. C. Davis, Oct. 1985.
 75. KYCHAKOFF, G., VAN CRUYNINGEN, I., PAUL, P. H. AND HANSON, R. K.: Applied Optics, in press.